Research paper

In-depth characterization of congenital Zika syndrome in immunocompetent mice: Antibody-dependent enhancement and an antiviral peptide therapy

Vidyleison N. Camargos [a], Giselle Foureaux [b], Daniel C. Medeiros [c], Vivian T. da Silveira [d], Celso M. Queiroz-Junior [b], Ana Luisa B. Matosinhos [d], André F.A. Figueiredo [e], Carla D.F. Sousa [a], Thaiane P. Moreira [a], Victória F. Queiroz [a], Ana Carolina F. Dias [a], Karina T.O. Santana [n], Ingredy Passos [n,o], Ana Luíza C.V. Real [f], Ludmila C. Silva [b], Flávio A.G. Mourão [c], Natália T. Wnuk [e], Milton A.P. Oliveira [g], Soraia Macari [h], Tarcília Silva [i], Gustavo P. Garlet [j], Joshua A. Jackman [k], Frederico M. Soriani [n], Márcio F.D. Moraes [c], Eduardo M.A.M. Mendes [c], Fabíola M. Ribeiro [f], Guilherme M.J. Costa [e], Antônio L. Teixeira [l], Nam-Joon Cho [k], Antônio C.P. Oliveira [d], Mauro M. Teixeira [m,n], Vivian V. Costa [n,o,*,1], Danielle G. Souza [a,*,1]

[a] Host-Microorganism Interaction Lab, Department of Microbiology, Institute of Biological Sciences, Universidade Federal de Minas Gerais, Belo Horizonte, MG, Brazil
[b] Transversal Biology Lab, Department of Morphology, Institute of Biological Sciences, Universidade Federal de Minas Gerais, Belo Horizonte, MG, Brazil
[c] Centre for Technology and Research in Magnetic-Resonance, Graduate Program in Electrical Engineering, Universidade Federal de Minas Gerais, Belo Horizonte, MG, Brazil
[d] Neuropharmacology Lab, Department of Pharmacology, Institute of Biological Sciences, Universidade Federal de Minas Gerais, Belo Horizonte, MG, Brazil
[e] Cellular Biology Lab, Department of Morphology, Institute of Biological Sciences, Universidade Federal de Minas Gerais, Belo Horizonte, MG, Brazil
[f] Neurobiochemistry Lab, Department of Biochemistry and Immunology, Institute of Biological Sciences, Universidade Federal de Minas Gerais, Belo Horizonte, MG, Brazil
[g] Department of Microbiology, Immunology, Parasitology and Pathology, Tropical Pathology and Public Health Institute, Federal University of Goiás, Goiania, GO, Brazil
[h] Department of Paediatric Dentistry and Orthodontics, Faculty of Dentistry, Federal University of Minas Gerais, Belo Horizonte, MG, Brazil
[i] Department of Oral Pathology and Surgery, Faculty of Dentistry, Federal University of Minas Gerais, Belo Horizonte, MG, Brazil
[j] Department of Biological Sciences, School of Dentistry of Bauru, São Paulo University, Bauru, SP, Brazil
[k] School of Materials Science and Engineering, Nanyang Technological University, Singapore
[l] Neuropsychiatry Program, Department of Psychiatry and Behavioural Sciences, McGovern Medical Houston, University of Texas Health Science Center at Houston, Houston, TX, USA
[m] Immunopharmacology Lab, Department of Biochemistry and Immunology, Institute of Biological Sciences, Universidade Federal de Minas Gerais, MG, Brazil
[n] Centre for Drug Research and Development of Pharmaceuticals, Institute of Biological Sciences, Universidade Federal de Minas Gerais, MG, Brazil
[o] Research Group in Arboviral Diseases, Department of Morphology, Institute of Biological Sciences, Universidade Federal de Minas Gerais, MG, Brazil

ARTICLE INFO

ABSTRACT

Background: Zika virus (ZIKV) infection during pregnancy may cause major congenital defects, including microcephaly, ocular, articular and muscle abnormalities, which are collectively defined as Congenital Zika Syndrome. Here, we performed an in-depth characterization of the effects of congenital ZIKV infection (CZI) in immunocompetent mice.

Methods: Pregnant dams were inoculated with ZIKV on embryonic day 5.5 in the presence or absence of a sub-neutralizing dose of a pan-flavivirus monoclonal antibody (4G2) to evaluate the potential role of antibody-dependent enhancement phenomenon (ADE) during short and long outcomes of CZI.

Findings: ZIKV infection induced maternal immune activation (MIA), which was associated with occurrence of foetal abnormalities and death. Therapeutic administration of AH-D antiviral peptide during the early stages of pregnancy prevented ZIKV replication and death of offspring. In the post-natal period, CZI was associated with a decrease in whole brain volume, ophthalmologic abnormalities, changes in testicular morphology, and disruption in bone microarchitecture. Some alterations were enhanced in the presence of 4G2 antibody.

Interpretation: Our results reveal that early maternal ZIKV infection causes several birth defects in immunocompetent mice, which can be potentiated by ADE phenomenon and are associated with MIA. Additionally, antiviral treatment with AH-D peptide may be beneficial during early maternal ZIKV infection.

* Corresponding authorst at: Departamento de Morfologia and Departamento de Microbiologia, respectively. Instituto de Ciências Biológicas, Universidade Federal de Minas Gerais, Avenida Antônio Carlos, 6627, Pampulha, CEP 31270-901, Belo Horizonte, MG, Brasil.
E-mail addresses: vivianvcosta@icb.ufmg.br (V.V. Costa), dani@icb.ufmg.br (D.G. Souza).
[1] Both are corresponding authors.

1. Introduction

Zika virus (ZIKV) infection emerged as a global public health threat that is associated with severe neurological complications. ZIKV is an arbovirus that belongs to the *Flaviviridae* family and is mainly transmitted to humans through the bite of infected *Aedes* mosquitoes. Vertical transmission in humans can result in early miscarriage or mild to severe birth defects, which include visual and hearing impairment [1]. The most severe outcome after congenital ZIKV infection (CZI) is severe microceph-aly and the long-term consequences of ZIKV infection has yet to be determined. The term Congenital Zika Syndrome (CZS) has been coined to describe the most significant and pathognomonic alterations observed after ZIKV infection of the foetus: microcephaly and one or more other complications, including vision and hearing impairment, as well as articular and musculoskeletal abnormalities [2,3].

Epidemiological and experimental studies suggest that maternal inflammation during pregnancy, due to infection or other causes, can elicit maternal immune system activation (MIA). MIA is considered a risk factor for neurodevelopmental and psychiatric disorders during adulthood, including schizophrenia, depression, and anxiety [4,5]. In this regard, CZS might not only be associated with the direct effects of the virus infection on the developing foetus but also to MIA in response to ZIKV infection, which could in turn trigger the development of several long-term harmful consequences and contribute to CZS pathogenesis [4].

Several hypotheses have been proposed to explain the relative frequent occurrence of CZS in the recent epidemics in Brazil, including the existence of environmental, socio-economic, and epidemiological factors [6,7]. In this context, one plausible hypothesis is the occurrence of antibody-dependent enhancement (ADE) of ZIKV infection [8]. This hypothesis, which remains to be proven, is based on the increased incidence of CZS in areas of co-circulation of ZIKV and all *Dengue virus* (DENV) serotypes during the latest epidemic that occurred in Brazil and the genomic similarity between those viruses. In this regard, it is also not known whether ADE could facilitate MIA occurrence.

Here, using an immunocompetent mouse model of CZI, we investigated the effects of ZIKV infection on embryonic development and its long-term consequences during adulthood. Our results reveal that early ZIKV exposure during pregnancy induces MIA, which is associated with foetal abnormalities in the offspring. Those effects during early neurodevelopment were followed by long-term consequences in adult offspring born from ZIKV-infected dams. We also demonstrate that acute and long-term functional consequences of infection were exacerbated in the presence of previous immunity, suggesting that ADE contributes to CZS aggravation in immunocompetent mice. Finally, therapeutic administration of a brain-penetrating antiviral peptide (AH-D) to ZIKV-infected dams resulted in reduction of viral loads in foetal brains and decreased the percentage of malformations in offspring, providing the first proof-of-concept that therapeutic treatment of pregnant women with antiviral compounds may alter the fate of ZIKV infection during pregnancy and prevent disease symptoms associated with CZS in offspring.

Research in context

Evidence before this study

It is known that *Zika virus* (ZIKV) infection during pregnancy can cause several birth defects to developing foetuses, and this disease state is termed Congenital Zika Syndrome (CZS). However, few studies have begun to investigate the potential long-term outcomes of affected offspring and possible pathogenic mechanisms. In addition, maternal immune activation (MIA) during pregnancy is associated with the development of neuropsychiatric diseases of offspring during adulthood. Thus, consequences of congenital ZIKV infection might not only be caused by pathological effects of the virus infection, but also due to maternal inflammatory mechanisms. Finally, a novel antiviral peptide called AH-D showed therapeutic activity against ZIKV in vivo. Therefore, the peptide's antiviral activity should be further tested in other pre-clinical models to evaluate its potential therapeutic use.

Added value of this study

Here, we demonstrated that ZIKV infection in immunocompetent mice induced relevant maternal and foetal abnormalities, which worsened in the presence of anti-flavivirus antibodies. During the post-natal period, several alterations in the offspring of ZIKV-infected dams were detected, some of which were enhanced by previous flavivirus immunity and affected several systems such as the brain, eyes, testes, and bones. Finally, we provided further evidence that AH-D peptide therapy can abrogate ZIKV replication in vivo during pregnancy and ameliorated foetal abnormalities caused by ZIKV infection.

Implications of all the available evidence

Our findings highlight several short- and long-term consequences of congenital ZIKV infection, which could be potential clinical outcomes that might be expected in individuals born from ZIKV-infected mothers, and finally support the feasibility of an antiviral peptide therapy to prevent adverse pregnancy outcomes induced by ZIKV infection. Taken together, the current results suggest that the general population and clinicians should remain vigilant of long-term, potentially harmful symptoms that may afflict apparently healthy children who were born from ZIKV-infected mothers.

2. Material and methods

2.1. Virus, cell culture and antibodies

A contemporary ZIKV strain from Brazil (HS-2015-BA-01 accession no. KX520666), isolated from the serum of an infected patient in Bahia state, Brazil, was propagated in *Aedes albopictus* C6/36 cell line. Stock virus from cell culture and viral loads obtained from maternal plasma and spleen samples were titrated in Vero cells (https://www.atcc.org/products/all/CCL-81.aspx) as previously described [9]. Plaques were detected after five days of infection. Monoclonal antibody 4G2 hybridoma was acquired from ATCC (https://www.atcc.org/Products/All/HB-112.aspx), and a mouse IgG2a isotype control mAb from Acris Gmbh was

used as a control. Antibodies used in immunostaining assays included anti-caspase-3 (Abcam 13585 1:200 for brain and retina analyses; Abcam IM-0035 1:100 for testicular analysis), anti-Iba-1/AIF1 (PA5–21274), Fluoro-Jade C® (Merk Millipore AG325), anti-NeuN (Abcam 104225), and anti-S100B (Abcam 41548).

2.2. Mouse experiments

C57BL/6 mice (8–12 weeks) were set up for timed-mating and inoculated at embryonic day (ED) 5.5 with 10^6 PFU/mouse of ZIKV or PBS (control) intraperitoneally (i.p) [10]. To evaluate the role of ADE in ZIKV infection, 10 μg of 4G2 or IgG2a (control group) were injected intraperitonealy (i.p) 24 h before ZIKV infection and every 48 h after the first dose in accordance with Costa et al. [9]

For MIA assays, baseline blood samples from pregnant dams were collected 24 h prior to infection and at 2 h and 24 h post infection (as described in Fig. 1), with spleen collection at the last time point (24 h). For embryonic analyses, pregnant dams were euthanized on ED 15.5 for maternal and foetal tissue extraction (as described in Fig. 2). For evaluating long-term effects, offspring were euthanized 12 weeks after birth (as described in Fig. 3). To evaluate the AH-D peptide therapy, the peptide (25 mg/kg via i.p route) was administered daily (as described in Fig. 7). Results shown are representative of at least 4 to 6 independent experiments in which at least one dam from each of the three experimental groups (PBS, ZIKV, and 4G2 + ZIKV) were performed simultaneously (biological replicates). All animal experiments were approved by the Ethics Committee on Animal Use (CEUA/UFMG), under protocol number 217/2017.

2.3. Real-time RT-PCR

RNA was isolated and amplified using a RNeasy Mini Kit and one-step Quantinova Probe RT-PCR kit, respectively, following the manufacturer's instructions (QIAGEN, Germany). The following primer pair and probe were used: Forward: CCGCTGCCCAACACAAG. Reverse: CCACTA ACGTTCTTTTGCAGACAT. Probe: AGCCTACCTTGACAAGCAGTCAGACA CTCA. Real Time RT-qPCR was performed in a 7500 Fast Real-Time PCR System (Applied Biosystems, USA) with the following steps: 45 °C for 5 min; 95 °C for 5 min; 40 cycles of 95 °C for 5 s, followed by 60 °C for 30 s. For generation of a semi-quantitative standard curve, RT-qPCR was performed using RNA extracted from a standard viral sample.

2.4. Elisa assays

The concentrations of the cytokines in maternal plasma, spleen, placenta, and foetal brain were measured by using the following commercially available mouse antibodies from DuoSet enzyme-linked immunosorbent kits (R&D Systems, Minneapolis, MN): CCL2/JE/MCP-1 (1:10; catalogue no. DY479), CCL3/MIP-1α (1:10; catalogue no. DY450), CCL4/MIP-1β (1:10; catalogue no. DY451), CCL5/RANTES (1:10; catalogue no. DY478), CXCL9/MIG (1:10; catalogue no. DY492), CXCL10/IP-10/CRG-2 (1:10; catalogue no. DY466), TNF-α (1:2; catalogue no. DY410), IFN-γ (1:10; catalogue no. DY1026), TGF-β (1:10; catalogue no. DY1679), IL-1β/IL-1F2 (1:2; catalogue no. DY401), IL-10 (1:10; catalogue no. DY417), IL-6 (1:10; catalogue n. DY406), and IL-17 (1:10; catalogue no. DY421).

2.5. Offspring neurodevelopment analysis

During offspring development, several behavioural analyses were performed on the same mice, with a one week intervals between each test. All parameters of behavioural tests were analysed by using Anymaze® software.

2.5.1. Sociability test

The sociability test was performed in accordance with Radyushkin et al. [11] An unknown juvenile mouse in the right or left social chamber was alternated between trials, in order to analyse possible effects of lateral preference. Tests were recorded by a video camera and the time spent in each chamber was analysed.

2.5.2. Y-maze

This test was used to evaluate the working memory of offspring. The test apparatus consisted of a Y-shaped maze with three identical arms. Entries and alternance between each arm were recorded by video camera. The test and analyses were performed, as previously described [12].

2.5.3. Elevated plus maze

This test was performed in accordance with Funchal and Dani [13]. Each mouse was recorded by video camera and the instinct of explore open and closed arms, meaning avoid or allow risk was observed. The amount of time and transitions between open and closed arms were analysed.

2.5.4. Open field test

Basal locomotion was evaluated by measuring the distance travelled by a mouse, and initial screening of anxiety-like behaviour was evaluated by the number of entries and amount of time in the center of the apparatus, as previously described [14].

2.5.5. Sucrose preference test

This test was performed to observe the behaviour of rodents, which prefer to ingest a sweet solution instead of water when given a choice between the two (sucrose preference score) [14,15]. A reduction in this preference is characterized by anhedonia, a depression-like behaviour.

2.5.6. Magnetic Resonance Imaging (MRI) analysis

A volumetric brain study was performed by MRI for female offspring after four, eight, and 12 weeks post-birth and for male mice at 12 weeks post-birth. MRI experiments were performed by using a 4.7 T NMR system (Oxford Systems, UK) that is controlled by a UNITY Inova200 imaging console (Varian, USA). The imaging protocol consisted of coronal T2-weighted (TR = 3000 ms, TE = 50 ms) spin echo multislice scans, with 20 contiguous 1 mm thick slices. Mice were anesthetized during the whole imaging procedure with halothane (4% induction, 1.5% maintenance doses) and oxygen (1.5 L/min) via a facial mask. All brain morphometric measurements were performed using the NIH ImageJ program. The total brain volume (mm^3) (7 sequential slices from +2.8 to −3.2 cm referenced from Bregma) was calculated by summing-up the area of each section (mm^2) multiplied by the slice thickness (1 mm).

2.5.7. Brain sections and staining

Mice (12 weeks) were euthanized and brains were then collected for several staining analyses. Brain samples were processed for routine haematoxylin and eosin (H&E) staining and evaluated histopathologically according to previously described criteria [16]. A researcher performed the histopathological score of cerebral cortex and meningeal inflammation in a blinded manner. Cerebral cortex was graded as follows: 0, no damage; 1, minimal tissue destruction and/or mild inflammation/gliosis; 2, mild tissue destruction and/or moderate inflammation/gliosis; 3, definite tissue destruction (neuronal loss and parenchymal damage) and intense inflammation; 4, necrosis. Meningeal inflammation was graded from 0 to 4: 0, no inflammation, and 1 to 4 corresponding to 1 to 4 cell layers, respectively. The sum of cerebral cortex and meningeal scores comprised the final score, up to 8 points.

For immunostaining analyses, brain samples were processed and sliced as previously described [17]. Slices of cortex were stained for microglia (Iba-1 staining), neurons (NeuN staining), and astrocytes
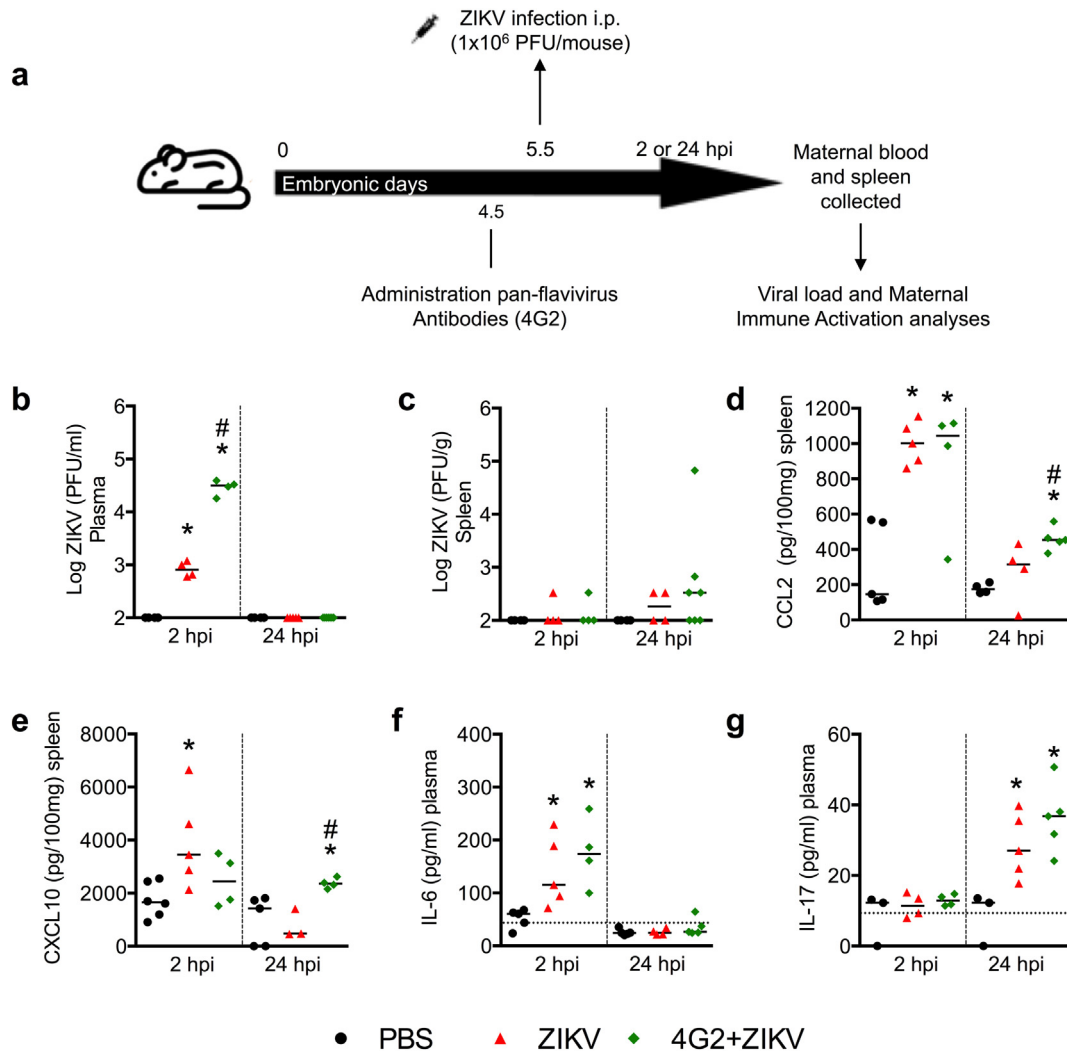
Fig. 1. ZIKV infection leads to maternal immune activation (MIA). Schematic representation of experimental strategy to evaluate maternal immune activation in mice (a). C57BL/6 pregnant mice were injected with PBS (black circles) or 10^6 PFU/mouse of Brazilian ZIKV strain (HS-2015-BA-01) on embryonic day 5.5 in the absence (red triangles) or presence (green lozenges) of anti-envelope monoclonal pan-flavivirus antibody (4G2). Spleen and plasma ($n = 4–6$) were collected 2 (left side of graphs) and 24 (right side of graphs) hours post infection (hpi) to determine the viral burden and inflammatory mediator levels by plaque formation assay and ELISA, respectively. Viral titters are shown as PFU per ml of plasma (b) or PFU per gram of splenic tissue (c). Concentrations of CCL2 (d) and CXCL10 (e) are expressed as picograms per 100 mg of splenic tissue and IL-6 (f) and IL-17 (g) as picograms per ml of plasma. All results are expressed as median and are representative of at least two independent experiments. *, $p < .05$ vs. PBS controls, #, $p < .05$ vs. ZIKV group, as assessed by Kruskal-Wallis followed by Dunn's post-test (b) or one-way ANOVA followed by Newman-Keuls post-test (d-g). Dashed lines in f and g are cytokine basal concentrations measured from plasma samples collected from the same animal 24 h prior to infection.

(S100β staining) following procedures supplied by the manufacturer (Vector Elite kit, Vector Laboratories, USA). Neurodegeneration was assessed by Fluoro-Jade C staining as described by Schmued et al. [18]

2.6. Offspring ophthamological analysis

2.6.1. Intraocular pressure measurement (IOP)

Between the 4th and 12th weeks post-birth, IOP measurements from offspring were performed weekly using an applanation tonometer Tono-Pen Vet (Reichert Technologies, USA) as previously described [19].

2.6.2. Histological analysis

The eyes were enucleated and histological sections were prepared according to Foureaux et al.[19] Retinal ganglion cells (RGC) counting were done by manually counting the whole extension of the retina. Caspase-3 expression in RGC was analysed by immunohistochemistry.

2.7. Offspring testicular analysis

2.7.1. Tissue preparation

After orchiectomy, testes were separated from epididymis, weighed, and cut longitudinally with a razor blade into small fragments. Testes were fixed for 24 h by immersion in Bouin's solution, embedded in glycol methacrylate (GMA - Leica historesin embedding kit) and in paraplast (Histosec® - Merck, USA) for histological, stereological, and immunostaining analyses.

2.7.2. Testis parenchyma and seminiferous tubule morphometrical analysis

Volume densities (%) of testicular tissue components were estimated by counting 6615 points over testis parenchyma [20]. Seminiferous tubule diameter and tubular lumen were measured, as described by Johnson and Neaves [21]. Seminiferous tubule morphology was classified according to its epithelium features, as follows: 1) presenting all germ cell types without apoptosis; 2) showing germ cell apoptosis/
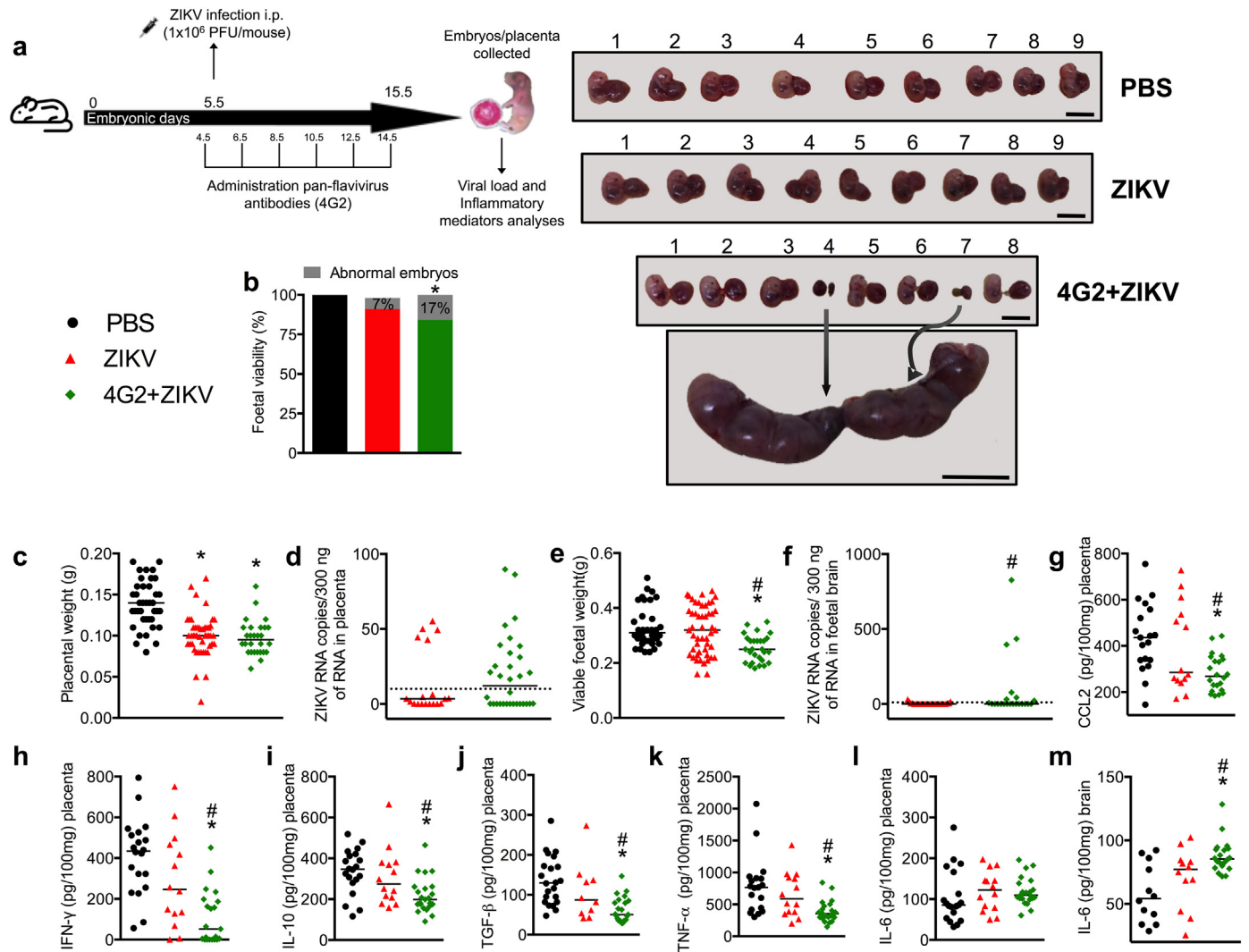
Fig. 2. Foetal viability, viral burden and inflammatory mediator alterations associated with ZIKV infection. Schematic representation of experimental strategy to evaluate the consequences of antibody-dependent enhancement on maternal ZIKV infection at the embryonic level (a). C57BL/6 pregnant mice were injected with PBS (black bar or circles) or 10^6 PFU/mouse of Brazilian ZIKV strain (HS-2015-BA-01) on embryonic day 5.5 in the absence (red bar or triangles) or presence (green bar or lozenges) of monoclonal pan-flavivirus antibody (4G2). After harvesting on ED 15.5 (n = 4–6; all foetuses and respective tissues from four-six pregnant dams), foetal malformations were registered (b) and viable foetuses (e) and placentas (c) were weighed. Representative pictures of litters from each group are shown on the right side of panel b, where two malformations are highlighted by arrows in a 4G2 + ZIKV animal-derived uterine horn. Scale bar represents 1 cm in all images. ZIKV RNA was quantified by qRT-PCR in placenta (d) and foetal brain (f). Inflammatory mediator concentrations were determined by ELISA in placenta (g-l) and foetal brain (m) and expressed as picograms per 100 mg of tissue. qRT-PCR results are expressed as the median of ZIKV RNA copies per 300 ng of sample RNA. ELISA results are expressed as median and are representative of at least two independent experiments. *, $p < 0.05$ vs. PBS controls, #, $p < 0.05$ vs. ZIKV group, as assessed by Fisher's exact test (b), Mann-Whitney test (f), or one-way ANOVA followed by Tukey (c and e) or Newman-Keuls post-test (g-m).

degeneration; 3) absence of germ cell layers; and 4) presenting retention of residual bodies. Thirty tubule cross-sections, randomly chosen, were evaluated per animal in these analyses.

2.7.3. Cell quantification

2.7.3.1. Germ cells. Cells present in stage VII of the seminiferous epithelium cycle were counted in ten seminiferous tubule cross-sections per mouse. Cell ratios/proportions were achieved from corrected counts according to Abercrombie [22] as modified by Amann [23].

2.7.3.2. Leydig cells. Leydig cell volume was obtained as described by Costa et al.[20] In addition, the Leydig cell number was estimated from the individual size and the total volume occupied by these cells in testis parenchyma.

2.7.4. Immunostaining analysis

Following standardized protocols [24], testicular serial sections (5 μm thick) were immunostained for Caspase-3. Reactions were visualized using biotin-conjugated secondary antibody in combination with Elite ABC Kit (Vector Laboratories, CA). In order to quantify the germ cell apoptotic index, fifteen seminiferous tubule cross-sections, randomly chosen, were evaluated for each animal. Data were expressed dividing the apoptotic germ cells number per seminiferous epithelium area. Analyses were conducted using Image J v.1.45 s software (Image Processing and Analysis, in Java).

2.8. Offspring bone analysis

2.8.1. Cell culture

Bone marrow cells (BMC) were obtained from the femurs of mice from PBS mock-infected and ZIKV-infected groups. Cells were
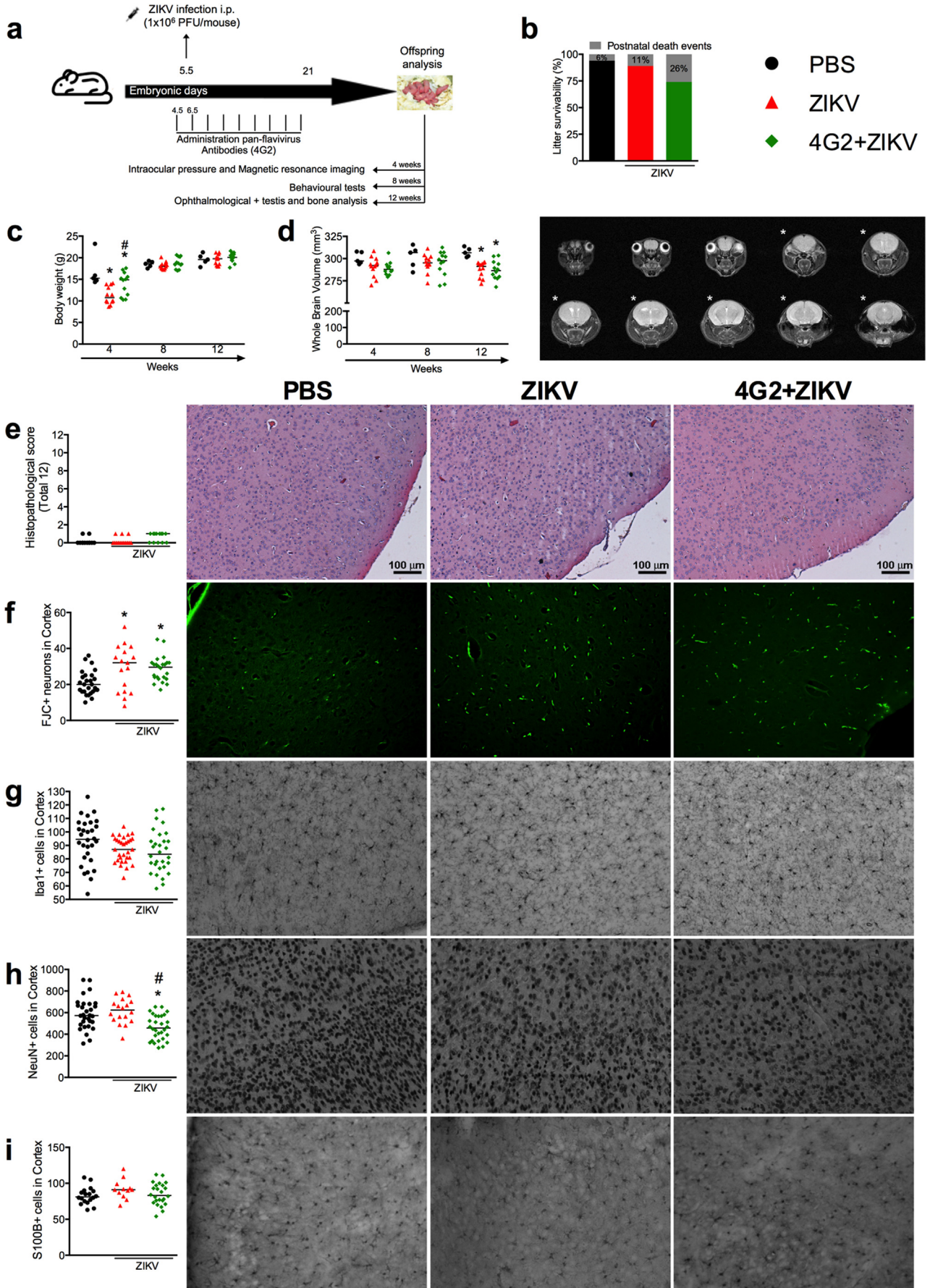
differentiated into osteoclasts and osteoblasts and analysed, as previously described [25].

2.8.2. Micro-computed tomography (micro CT) analysis

Trabecular microarchitecture and bone density within the metaphyseal region of distal femurs were quantified using micro CT according to Macari et al.[25]

2.8.3. Histomorphometry

Measurements were performed at the distal femur excluding the growth plate where the distal metaphysis was performed, as previously described [25] according to international standards. H&E staining was used for measuring the density of osteocytes per trabecular bone area, tartrate resistant acid phosphatase (TRAP; Sigma-Aldrich, USA) for osteoclasts TRAP positive analysis and Masson's Thricrome staining used for osteoblasts per trabecular bone perimeter.

2.8.4. mRNA extraction and qPCR

For quantitative PCR (qPCR) analysis, we extracted the mRNA from femur specimens with Trizol and column purification (RNeasy Mini Kit, Qiagen Inc., USA). We prepared complementary DNA with Superscript Vilo Master Mix (Thermo Fisher Scientific, USA) and performed qPCR analysis on a Light Cycler 480 (Roche Applied Science) with the following target genes: RANK (*Tfnrsf11a*), RANKL (*Tnfsf11*), osteoprotegerin (OPG, *Tnfrsf11b*), RANKL/OPG ratio, TNF-α (*Tnf*), and interleukin-6 (*il6*). For calculation of the relative gene expression, we normalized data to the gene encoding glyceraldehyde-3-phosphate dehydrogenase (GAPDH) and quantified the results using the cycle threshold (Ct) method and 2-ΔΔCt calculation [25].

2.9. Statistical analyses

Data were tested for normality and homoscedasticity of the variances. Quantitative data were presented as median values, except for IOP measurements, which were displayed as the mean ± SEM (standard error of the mean). Analyses were conducted using the PRISM v7.0 software program (GraphPad Software, Inc). Data were analysed using different *t*-tests as appropriate. An unpaired parametric t-test for comparison between two groups, or a one- or two-way ANOVA for comparisons between three groups was used, followed by the Newman-Keuls test in the case of data with a normal distribution, or the Kruskal-Wallis followed by Dunn's test in the case of nonparametric data. Fisher's exact test was used to compare categorical variables. Differences were considered statistically significant at $p < .05$.

3. Results

3.1. Zika virus infection induces maternal immune activation

Recently, Rathore et al. [26] demonstrated the enhancement capacity of subneutralizing doses of either immune DENV serum or 4G2 antibody, during ZIKV infection in immunocompetent dams. In the present work we performed similar experiments by using subneutralizing doses of the 4G2 pan-flavivirus antibody and aimed to evaluate the short- and long-term consequences of the antibody-dependent enhancement

phenomenon on ZIKV-infected offspring. In this study, a subneutralizing dose of 4G2 antibody refers to a dose that is sufficient to allow virus-complex formation but not to neutralize the virus. First, the neutralizing capacity of 4G2 antibody against ZIKV was evaluated in vitro using the human monocyte cell line - THP-1 ATCC® TIB-202™ (data not shown). Next, to evaluate the ability of ZIKV to induce Maternal Immune Activation (MIA), pregnant C57BL/6 mice were infected with ZIKV on embryonic day (ED) 5.5 and samples were collected at 2- or 24-h post-infection (hpi) for measurement of viral loads and systemic inflammatory mediators. In parallel, to emulate a secondary infection in vivo, pregnant mice were injected with a sub-neutralizing dose of 4G2 24 h before ZIKV infection (Fig. 1A). Throughout the experiments, the negative control group received PBS solution (PBS group) and the positive control group received an isotype control antibody (IgG2a) with no specificity against ZIKV (ZIKV group). 10^3 viable particles were recovered from the plasma of isotype-treated, ZIKV-infected dams 2 hpi and 10^5 viable particles from 4G2-treated dams at the same time point (Fig. 1B). At 24 hpi, no viable virus was detected in any group. In spleen, viral loads were similar between ZIKV and 4G2-ZIKV dams at both time points (Fig. 1C).

In the ZIKV-infected group, we also detected increased levels of CCL2 and CXCL10 in spleen only 2 hpi while, in the 4G2 + ZIKV group, a higher concentration of CCL2 occurred at both time points and there was a delay in CXCL10 production with an increase observed at 24 hpi (Fig. 1D-E). The increase in the levels of IL-6 and IL-17 presented the same profile in both groups: an increase in IL-6 at 2 hpi and increase in IL-17 at 24 hpi in the plasma of infected mice (Fig. 1F-G). Of note, there were no changes in the levels of other cytokines evaluated in spleen (Fig. S1A—I) and plasma (Fig. S2) in both infected-groups, as compared to PBS-injected controls at both time points.

3.2. Congenital Zika virus infection causes placental and foetal damage, which are aggravated by pre-treatment with 4G2 antibody

To investigate the consequences of ADE on ZIKV infection at the embryonic level, the experimental design was performed as presented in Fig. 2A. Briefly, pregnant dams received subneutralizing doses of 4G2 antibody (10 μg) 24 h before ZIKV inoculation and every 48 h after the first antibody injection until ED 14.5 as described in [9]. To ensure that consecutive intraperitoneal injections would not induce any additional distress to the mother or offspring, the same experimental protocol, including contention methods and antibody inoculation, was applied for both negative control and ZIKV-infected groups, which received PBS and IgG2a antibody, respectively. Based on this format, our results demonstrate that ZIKV infection resulted in a reduction of about 7% in foetal viability (Fig. 2B) when compared to PBS controls. Foetal demise was about 17% in the 4G2 + ZIKV group during the same period (Fig. 2B). The placental weight was decreased in both infected-groups in comparison to the PBS group (Fig. 2C). In addition, detection of ZIKV RNA was similar between the ZIKV and 4G2 + ZIKV groups in the placenta (Fig. 2D). A more pronounced decrease in whole foetal body weight from viable embryos was observed in the 4G2 + ZIKV group when compared to the offspring of PBS-injected and ZIKV-infected dams (Fig. 2E). Accordingly, a higher number of ZIKV-RNA positive samples were detected in foetal brains in the 4G2 + ZIKV group in comparison to the

Fig. 3. Administration of 4G2 contributes to the exacerbation of persistent neuropathological outcomes in offspring born from ZIKV-infected dams. Schematic representation of experimental strategy to evaluate the long-term consequences of ZIKV infection during pregnancy and exacerbation of potential abnormalities related to CZS by antibody-dependent enhancement of ZIKV infection (a). C57BL/6 pregnant mice were injected with PBS (black bar or circles) or 10^6 PFU/mouse of Brazilian ZIKV strain (HS-2015-BA-01) on embryonic day 5.5 in the absence (red bar or triangles) or presence (green bar or lozenges) of monoclonal pan-flavivirus antibody (4G2). Pregnant dams were accommodated in separate cages until natural litter were born. Then, partial or total postnatal litter deaths were registered (b). Female offspring ($n = 6$; one or two mice from six different dams) were weighed (c) and brain volume was quantified by magnetic resonance imaging (d). Left panel in (d) represents sequential brain images and asterisks indicate which slices were used to determine the brain volume. Animals were euthanized, their brains collected and stained by haematoxylin and eosin (e), Fluoro-Jade C (f; neurodegeneration), or immunohistochemistry using anti-Iba1 (g; microgliosis), anti-NeuN (h; neuron counting), or anti-S100B (i; astrocyte counting) antibodies. Two brain slices of five different mice (from five different dams) per group were used. Three representative images of each section (right side of graphs) were quantified using ImageJ software and results are expressed as the median of all cell counts per group (e-i). Magnification, 200×. Scale bar, 100 μm. *, $p < .05$ vs. PBS controls. #, $p < .05$ vs. ZIKV group, as assessed by two-way ANOVA followed by Tukey post-test (c-d) or one-way ANOVA followed by Newman-Keuls post-test (f and h).

mice that were only infected with ZIKV (Fig. 2F). However, no detectable viral particles were recovered from any group.

There were similar levels of the inflammatory mediators CCL2, IFN-γ, IL-10, TGF-β, TNF-α, and IL-6 (Fig. 2G-L) in the placenta of non-infected and ZIKV-infected dams. Of note, no alterations on baseline cytokine levels of mice that received IgG2a or 4G2 antibodies in comparison to PBS-injected controls were observed (data not shown). Interestingly, the levels of all inflammatory mediators were lower in the placenta of the 4G2 + ZIKV group when compared to PBS and ZIKV groups (Fig. 2G-K), with the exception of IL-6 (Fig. 2L). There were no changes in the concentrations of CCL5, IL-1β, IFN-α, or IFN-β in the placenta (Fig. S3A-D). Of note, IL-6 levels were elevated in the foetal brain of 4G2 + ZIKV, but not in the ZIKV group (Fig. 2M). While CCL2, IL-10, IFN-γ, and TGF-β levels were reduced in the brains of the ZIKV group (Fig. S3I-L), only the latter two cytokines were also downregulated in the brain of 4G2 + ZIKV foetuses (Fig. S3K-L). No alterations in CCL5, IL-1β, IFN-α, IFN-β, or TNF-α levels were found in the brains of offspring (Fig. S3E—H, M). Overall, the administration of a subneutralizing dose of 4G2 to pregnant dams resulted in a greater frequency of viral infections and enhanced foetal demise, and these responses were associated with inflammatory hyporesponsiveness in the placenta as well.

3.3. Congenital Zika virus infection results in neuropathological abnormalities in the offspring of ZIKV-infected dams

Next, to investigate the long-term consequences of ZIKV infection during pregnancy and whether treatment with 4G2 could also exacerbate potential abnormalities related to CZS from birth to adulthood, the natural birth of the pups was facilitated as demonstrated in Fig. 3A. Pregnant dams were monitored daily after ZIKV infection by means of weight measurements and appearance of clinical signs. The results revealed no change in weight gain (Fig. S4A) or appearance of clinical symptoms until litter birth, in all evaluated groups. However, a reduction in offspring survival was observed in the ZIKV group (about 11%) and the 4G2 + ZIKV group (26%), compared to the PBS group (6%) (Fig. 3B).

Whole brain volume, which is an indicator of brain development, was measured by magnetic resonance imaging (MRI) from the 4th to the 12th week of life (Fig. 3D). The results revealed a reduction in overall body weight at the 4th week of life for female offspring of ZIKV-infected dams (Fig. 3C), although the brain volume at this time point was similar among the tested groups (Fig. 3D). Thereafter, at the 8th and 12th weeks of life, the body weight of female offspring from ZIKV-infected dams became similar to those born from dams in the PBS control group (Fig. 3C). However, there were significant changes in brain volume in both infected groups at the 12th week after birth, as compared to PBS controls. Similar results were found in the group of male mice who has been subjected to MRI analysis at the 12th week after birth (Fig. S4B—C).

Histopathological analyses of brain slices from 12-week-old offspring showed no gross changes in the brains of ZIKV and 4G2 + ZIKV groups in comparison to PBS controls (Fig. 3E). Notably, there was increased neurodegeneration, as assessed by Fluoro-Jade C staining, in samples from the offspring of ZIKV-infected and 4G2 + ZIKV dams (Fig. 3F). However, there were no changes in the number of IBA1+ (Fig. 3G) and S100B+ (Fig. 3I) cells in the control or infected mice. The number of NeuN+ neurons was reduced in the cortex of 4G2 + ZIKV offspring in comparison to PBS and ZIKV littermates (Fig. 3H).

Next, we performed a series of cognitive and behavioural tests on male offspring between the 8th and 12th weeks of life (Table S1). Cognitive tests evaluating sociability (sociability test), anxiety (elevated plus maze and open field tests), and working memory (Y-maze test) presented similar results in all groups of mice. Further analysis also revealed the absence of changes in motor locomotion (open field test) and depression (sucrose preference test) in all groups.

3.4. Congenital Zika virus infection results in ophthalmological abnormalities in the offspring of ZIKV-infected dams

Our results showed a slight increase in the IOP values of the ZIKV-infected group in comparison to the control group (Fig. 4A). Strikingly, mice from the 4G2 + ZIKV group displayed even higher IOP levels at all evaluated time points. Next, we collected the eyes at week 12 to examine the number of Retinal Ganglion Cells (RGC) (Fig. 4B). Even though RGC counts from the animals in the PBS and ZIKV-infected groups showed similar cell numbers, there was a significant reduction in the RGC counts in the 4G2 + ZIKV group when compared to the PBS control. The reduction in RGC counts was associated with an increase in the number of cells that stained positive for caspase-3 (Fig. 4C).

3.5. Congenital Zika virus infection results in testicular abnormalities in the offspring of ZIKV-infected dams

Important histological testicular parameters were evaluated in control (Fig. 5A), ZIKV (Fig. 5B), and 4G2 + ZIKV (Fig. 5C) groups. There were no detectable changes in macroscopy or weight of the testes of offspring from infected or non-infected dams (Fig. 5D). However, there was a significant reduction in the density of testicular components, including reduction in seminiferous tubule volume, tubular diameter, and tubular lumen (Fig. 5E-G) in the infected groups when compared to the control and ZIKV-infected groups. Indeed, ZIKV and 4G2 + ZIKV groups presented important morphological alterations in seminiferous tubules when compared to non-infected littermates (Fig. 5B1, C1, H). About 40% of the seminiferous tubules showed some altered features, as shown by seminiferous epithelium degeneration, absence of some germ cell types, and retention of residual bodies (Fig. B2, C2, I). Indeed, Sertoli cell efficiency, estimated by the number of round spermatids per Sertoli cell, was reduced in the 4G2 + ZIKV group (Fig. 5J). The meiotic index, measured as the number of round spermatids produced per pachytene primary spermatocyte (Fig. 5K), was also reduced in the both infected groups when compared to the control group. Accordingly, a higher frequency of Caspase-3-positive cells per area of seminiferous epithelium was found in the ZIKV-infected group, although it was not different in the 4G2 + ZIKV group (Fig. 5L-O). Intertubular testis analysis revealed no significant alterations with respect to blood vessels (Fig. S5I) and Leydig cells (Fig. S5A—H).

3.6. Congenital Zika virus infection affects bone quality in the offspring of ZIKV-infected dams

Femurs from adult offspring born from PBS, ZIKV, and 4G2 + ZIKV-infected dams were collected and analysed by micro-computed tomography (Micro CT) analysis. Our results show that ZIKV infection induced marked bone loss in the femur of adult litters, as shown by a significant decrease in various bone parameters, including bone mineral density (BMD), percentage of trabecular bone volume/total volume (BV/TV%), trabecular thickness (Tb.Th), trabecular number (Tb.N) and increase in the structure model index (SMI) (Fig. 6). These changes were comparable in the ZIKV and ZIKV+4G2 groups. Moreover, there was no difference in trabecular separation (Tb.Sp) in the bones of adult offspring from infected or non-infected mice (Fig. 6F).

Fig. 6K shows representative photomicrography from osteoclasts (top panel), osteoblasts, and osteocytes (bottom panel) in the offspring of control and infected mice at 12 weeks of age. Osteoclasts were identified as TRAP-positive, osteoblasts were recognized in sections by their size, shape, and position in bone (black arrows, bottom panel), and osteocytes were surrounded by bone in the trabecular bone of the femur (red square, bottom panel). In agreement with the Micro CT analysis, there was as an increase in number of osteoclasts (Fig. 6H) and osteocytes (Fig. 6I) in both infected groups. The number of osteoblasts was only increased in the 4G2 + ZIKV group (Fig. 6J). There was a similar
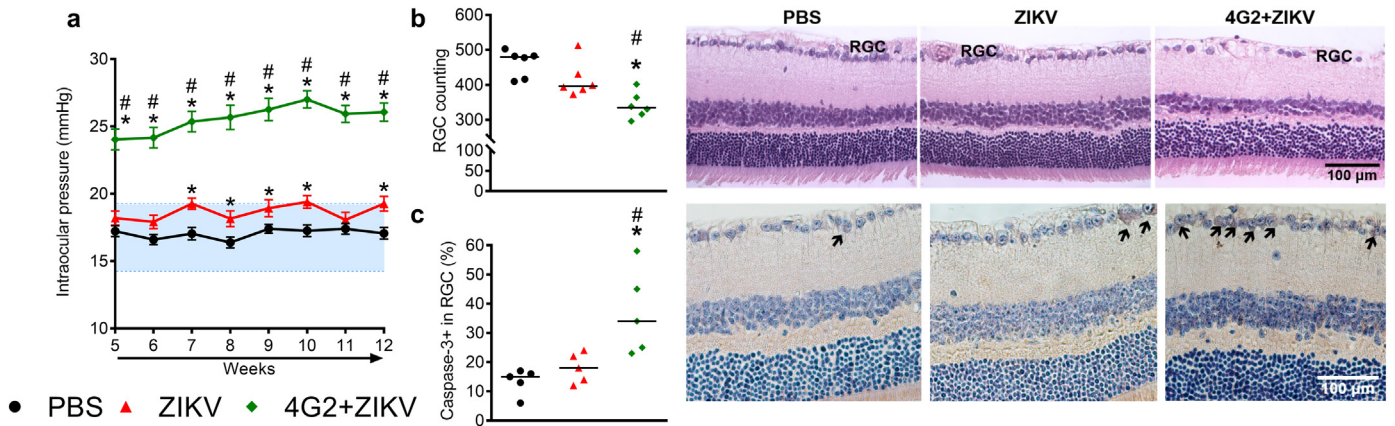
Fig. 4. Ophthalmological abnormalities of offspring associated with ZIKV infection. C57BL/6 pregnant mice were injected with PBS (black circles) or 10^6 PFU/mouse of Brazilian ZIKV strain (HS-2015-BA-01) on embryonic day 5.5 in the absence (red triangles) or presence (green lozenges) of monoclonal pan-flavivirus antibody (4G2). Offspring born from injected dams were analysed. Intraocular pressure was measured weekly for offspring from the 4th to 12th week of age (a), where the highlighted area in blue indicates normal values of IOP in C57BL/6 mice. After euthanasia, eyes ($n = 5$–6; one mouse from five or six different dams) were enucleated for Retinal Ganglion Cell counting (b) and caspase-3 immunohistochemistry analysis (c). In representative images of retinas, RGC layer are specified in (b) and caspase-3 positive cells are indicated by arrows in (c). Magnification, 400×. Scale bar = 100 μm. IOP results are expressed as mean ± SEM and cell counts are shown as median. *, $p < .05$ vs. PBS controls, #, $p < .05$ vs. ZIKV group, as assessed by two-way (a) or one-way ANOVA followed by Newman-Keuls post-test (b-c).

increase in RANKL/OPG ratio and IL-6 mRNA expression (Fig. 6L and M) in the femur of offspring born from both groups. There were no significant differences in RANK or TNF-α (Fig. 6 N-O) mRNA expression in all groups.

In vitro experiments conducted with BMCs from the femurs of PBS and ZIKV-infected mice revealed a decrease in osteoclast viability and enhanced osteoclast differentiation as determined by an increase in MTT- and TRAP-positive cell numbers, respectively, in the ZIKV-infected group when compared to the PBS control (Fig. S6A—C). Enhanced osteoblast activity, as assessed by an increase in alizarin red absorbance, was also detected in BMCs obtained from ZIKV-infected animals in comparison to PBS controls (Fig. S6D-E).

3.7. Therapeutic administration of an antiviral peptide (AH-D) decreases the frequency of viral infection and reduces foetal death

In order to explore whether the AH-D peptide could prevent viral replication and foetal death, the peptide was therapeutically administered daily starting three days after infection of dams (Fig. 7A). As mice subjected to 4G2 treatment had more severe disease in some parameters, this model was chosen for evaluating the therapeutic treatment as shown in Fig. 7A. Fig. 7B shows that, while seven of 54 pups (13%) from vehicle-treated dams presented ZIKV RNA copies that were recovered from the brain, therapeutic administration of AH-D peptide prevented ZIKV RNA detection in all of the 36 pups (Fig. 7B). Accordingly, the frequency of foetal demise dropped from 21% in vehicle-treated to 10% in AH-D peptide-treated dams (Fig. 7C). However, viral replication inhibition by AH-D peptide therapy was insufficient by itself to prevent the reduction of placental and whole foetal weight induced by ZIKV infection (Fig. 7D-E).

4. Discussion

The major findings of this study were: i) congenital ZIKV infection of immunocompetent adult pregnant mice causes transient systemic inflammation (MIA), placental infection, and foetal demise; ii) administration of a subneutralizing dose of a pan-flavivirus antibody before infection appears to enhance congenital ZIKV infection, as seen by prolonged MIA, enhanced frequency of brain infection, and foetal demise, along with causing placental inflammatory hyporesponsiveness; iii) congenital ZIKV infection caused major changes in the brain, eyes, testes, and bones of the adult offspring; iv) changes in the testes and bone of offspring of infected dams were not aggravated by previous

administration of 4G2 antibody whereas changes in brain and eye became more pronounced; v) treatment with an antiviral peptide decreased the frequency of brain infection and foetal demise in a mouse model of CZI.

Epidemiological evidence implicates that the activation of the maternal immune system during pregnancy can be triggered by several types of stimuli, including infectious agents such as TORCH pathogens, leading to the development of neuropsychiatric disorders in adulthood [4]. Here, we demonstrated that congenital ZIKV infection resulted in MIA as demonstrated by elevated levels of proinflammatory mediators, such as CCL2, CXCL-10, IL-6, and IL-17, in infected dams. Interestingly, in the presence of 4G2, there was a prolonged detection of chemokines and increased viral load in maternal plasma, suggesting that ADE could contribute to the exacerbation of MIA during congenital ZIKV infection. Accordingly, production of IL-17 driven by IL-6 plays a key role in MIA as demonstrated in previous studies [27–29]. Indeed, a single injection of IL-6 to pregnant mice has been shown to be sufficient to induce MIA and resulted in behavioural alterations in offspring, which were prevented by an IL-6 blockade in vivo. [30]

In accordance with recently work published by Rathore et al. [26], we did not detect increased ZIKV RNA copies in the placenta of the 4G2 + ZIKV group compared to isotype-matched controls, however, higher viral loads in the foetal brain of the 4G2 + ZIKV group was observed. Analysis of inflammatory mediators in placentas revealed a general placental hyporesponsiveness profile that was characterized by reduced levels of cytokines in the 4G2 + ZIKV group. By contrast, elevated levels of IL-6 in the brain of the offspring born from those dams were found and were associated with a higher frequency of offspring malformations, providing evidence of the role played by ADE in the enhancement of ZIKV infection and suggesting that there is induction of neuroinflammation on the offspring. Accordingly, several in vitro and experimental studies in rodents have supported the occurrence of the ADE phenomenon during ZIKV infection [26,31–36]. However, others have indicated a lack of cross-reaction or even protection from ZIKV infection after DENV infection in experimental models and clinical-epidemiological findings [37–42]. Indeed, in the context of MIA, there is evidence that elevated levels of pro-inflammatory cytokines negatively impact the development cortical neuron dendrites, causing a neuropathy similar to schizophrenia [43]. Taken together, our results support the idea that ADE contributes to the enhancement of ZIKV infection and MIA, which could eventually lead to the abnormal pathology associated with CZS.
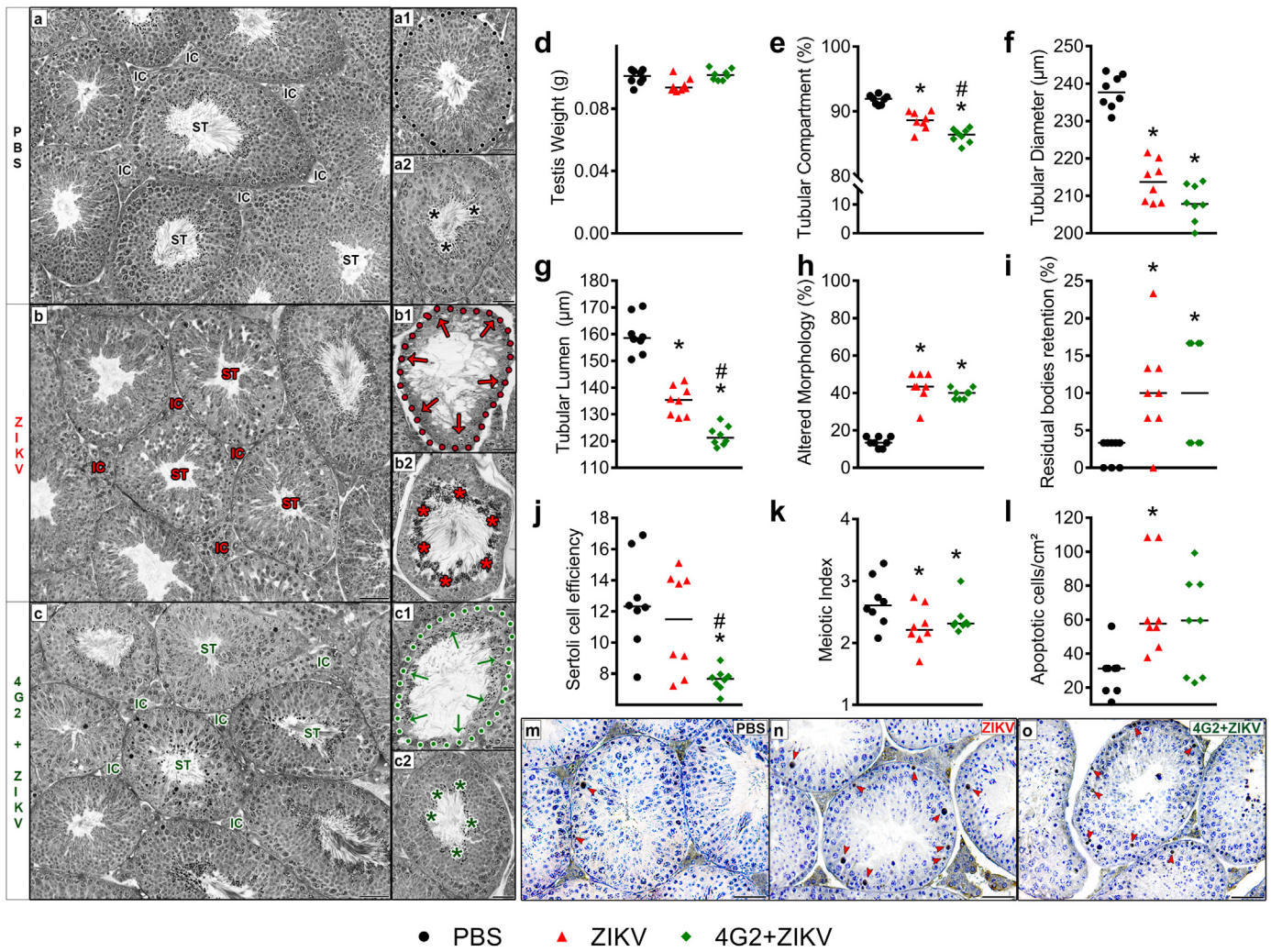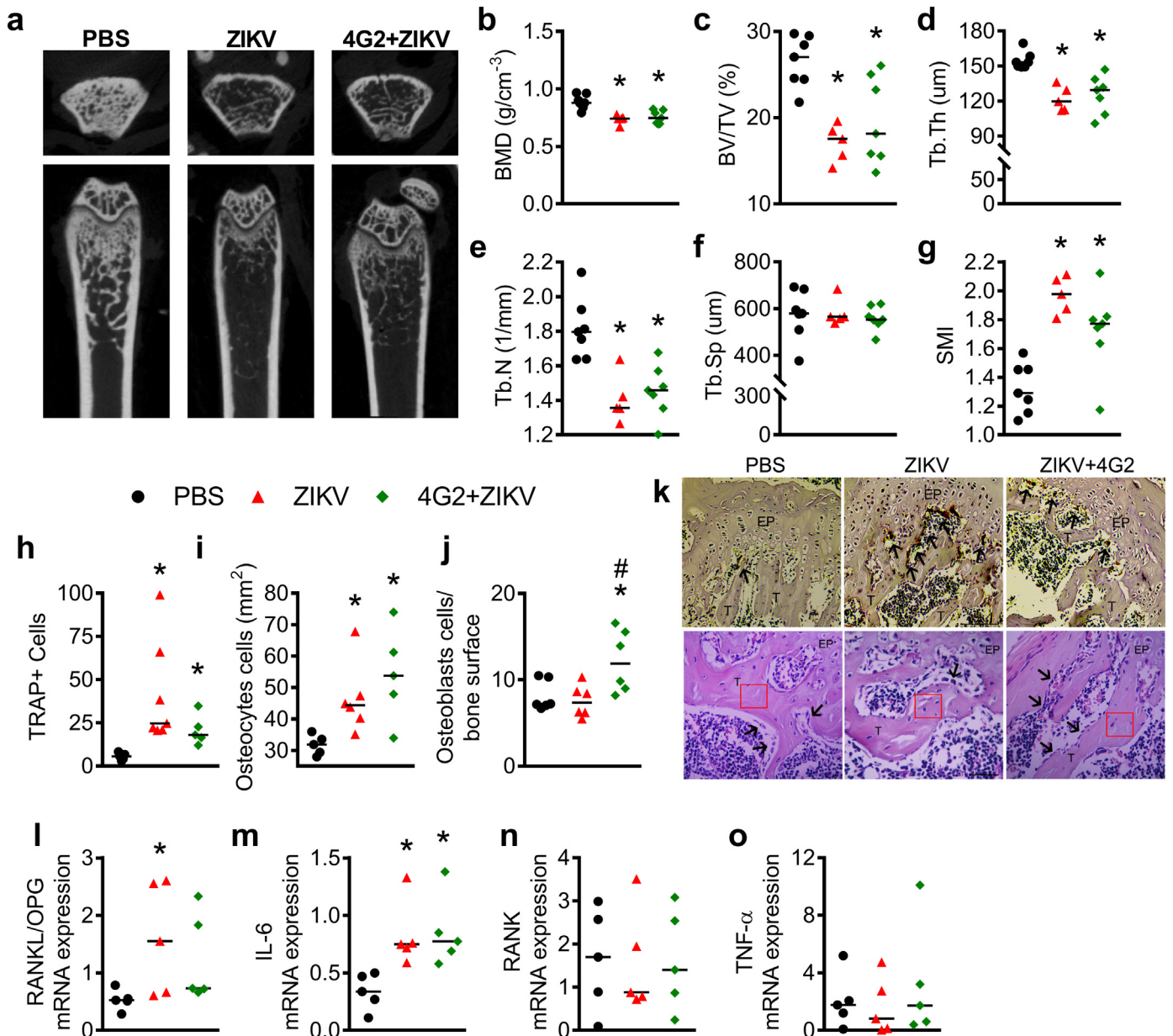
Fig. 5. Changes in the testis tubular compartment of offspring associated with ZIKV infection. C57BL/6 pregnant mice were injected with PBS (black circles) or 10^6 PFU/mouse of Brazilian ZIKV strain (HS-2015-BA-01) on embryonic day 5.5 in the absence (red triangles) or presence (green lozenges) of monoclonal pan-flavivirus antibody (4G2). Offspring born from injected dams were analysed. After euthanasia at 12 weeks-of-age followed by orchiectomy (n = 5; at least one random animal from five different dams in each group), testis were weighed (d) prior to morphometrical analyses, which included the proportion of tubular compartments (e), tubular diameter (f), and tubular lumen (g), morphological alterations (h), such as seminiferous epithelium degeneration (arrows in b1 and c1), absence of germ cell types (b1, c1), and increased retention of residual bodies (asterisks in b2 and c2; (i), Sertoli cell efficiency (j), meiotic index (k), and prevalence of caspase-3 positive cells (l); red arrowheads in (m-o) per area of seminiferous epithelium. Images: IC = interstitial compartment; seminiferous tubules (ST); cross-sections (dotted line). Magnification = 200×. Scale bar (black lines) = 50 μm. Results are expressed as median values. *, p < .05 vs. PBS controls, #, p < .05 vs. ZIKV group, as assessed by one-way ANOVA followed by Tukey post-test (e-l).

While the short-term impact of congenital ZIKV infection has been investigated in some detail [1,44–48], only a few studies have started to investigate the long-term consequences of CZS in offspring. In this context, Satterfield-Nash and colleagues [49] followed-up on the health and development of nineteen children with a confirmed microcephaly diagnosis at birth until 19–24 months of age. The results revealed that most of these children presented severe motor impairment, seizure disorders, hearing and vision abnormalities, and sleep difficulties. Accordingly, using Swiss mice inoculated with ZIKV three days after natural birth, the authors showed the occurrence of postnatal microcephaly and behavioural changes during adulthood, as evidenced by increased seizure episodes along with motor and cognitive dysfunctions in adult offspring [50]. In this study, we demonstrated that congenital ZIKV infection was associated with a reduction in brain volume, increased neurodegeneration, and reduced neuronal cell counts in adult offspring born from ZIKV and 4G2 + ZIKV infected groups, suggesting an impairment in brain development at adulthood. Our findings agree well with several other experimental analyses conducted in newborn mice in which cortical disorganization after ZIKV infection was also observed

[44,51–53]. However, maternal infection on embryonic day (ED) 5.5 was not able to induce significant behavioural abnormalities in adult offspring. A previous study also demonstrated that maternal ZIKV infection of AG129 mice on ED 7.5 did not result in any motor or cognitive deficits in adulthood [54]. These results lead to an important insight about the "vulnerability window", during which stage there is a greater likelihood of infection leading to long-term development of neurological-like symptoms and suggesting that, during the initial stage, the placenta plays a more important role due to increased exchange between the mother and foetus.

ZIKV infection has also been shown to be associated with substantial ophthalmological abnormalities both in infants with confirmed microcephaly diagnosis and in children with a normal cephalic perimeter [55,56]. Here, we demonstrated that ADE and its associated MIA could contribute to the exacerbation of ophthalmological abnormalities induced by congenital ZIKV infection. This change was associated with a massive reduction in RGC numbers secondary to apoptosis events, as demonstrated by an increase in Caspase-3 staining. Our results are in accordance with previous studies that showed that direct intrauterine
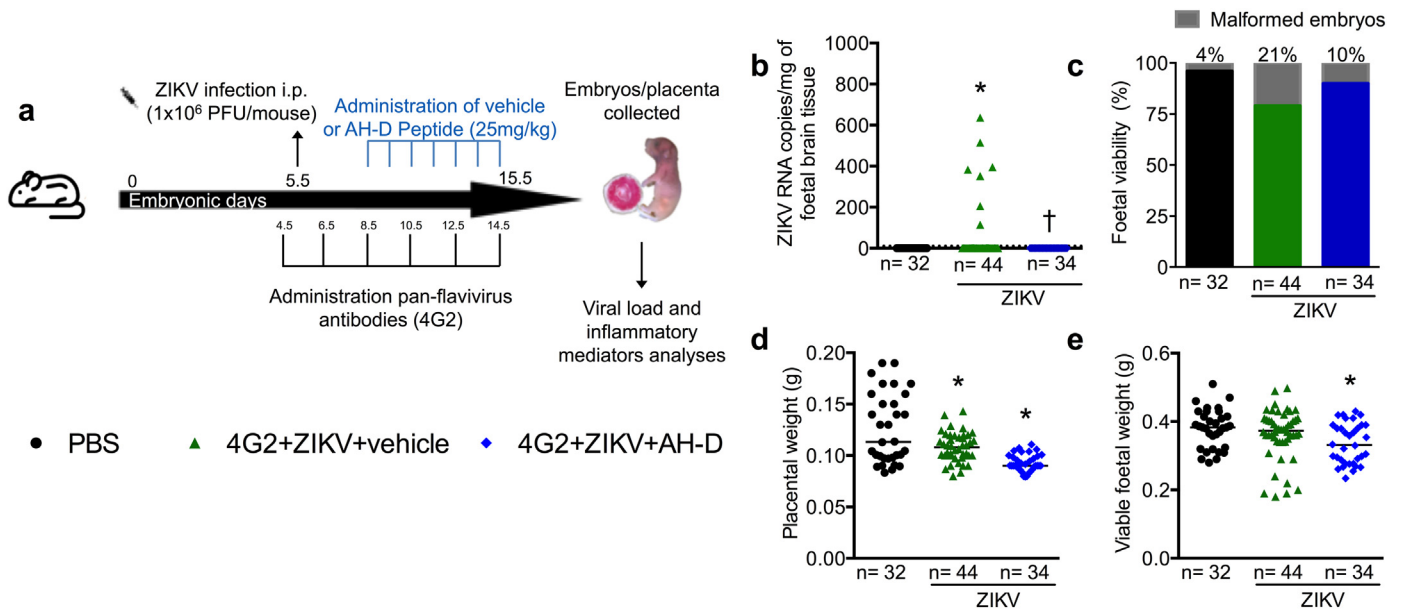
Fig. 6. Bone alterations in offspring associated with ZIKV infection. C57BL/6 pregnant mice were injected with PBS (black bar or circles) or 10^6 PFU/mouse of Brazilian ZIKV strain (HS-2015-BA-01) on embryonic day 5.5 in the absence (red bar or triangles) or presence (green bar or lozenges) of monoclonal pan-flavivirus antibody (4G2). Offspring born from injected dams were analysed. After euthanasia at 12 weeks-of-age, femurs were collected and analysed by micro-computed tomography (micro CT) and images are shown in (a), and the analysed parameters included: bone mineral density (b; BMD, g/cm^3), percent bone volume (c; BV/TV %), trabecular thickness (d; Tb.Th, μm), trabecular number (e; Tb.N, 1/mm), trabecular separation (f; Tb.Sp, μm), and structure model index (g; SMI). Femur bone loss was evaluated by osteoclasts, osteocytes, and osteoblast counting (h-k). Osteoclasts representative photomicrography (k, upper panel; black arrows indicate TRAP-positive osteoclasts, T – trabecular bone, EP - epiphyseal disk). Magnification: 20×. Scale bar = 100 μm. Osteoblast representative photomicrography (k, bottom panel; black arrows demonstrate osteoblasts in contact with trabecular bone, T - trabecular bone, EP - epiphyseal disk; red square – area where osteocytes were counted). Magnification: 40×. Scale bar = 50 μm. mRNA expression of (l) Receptor activator of nuclear factor kappa-B ligand/osteoprotegerin ratio (RANKL/OPG), (m) interleukin-6 (IL-6), (n) Receptor activator of nuclear factor kappa-B (RANK), and (o) tumour necrosis factor (TNF) in the femur of offspring. Results are expressed as the median. *, p < .05 vs. PBS controls, #, p < .05 vs. ZIKV group, as assessed by one-way ANOVA followed by Tukey post-test (b-e, g-j, and l-m).

ZIKV inoculation to immunocompetent C57BL/6 dams or pregnant rhesus macaque presented ocular abnormalities [52,57]. Overall, the findings indicate that congenital ZIKV infection is associated with long-term ophthalmological impairment that may progress to chronic conditions leading to an irreversible impact on visual field loss.

Here, we identified important morphological alterations in the tubular compartment of testis in offspring born from ZIKV-infected dams. Recent studies have shown that ZIKV has tropism to several cell types such as spermatogonia, primary spermatocytes, and Sertoli cells [58–61]. Marked germ cell apoptosis and detachment of Sertoli cells from the basement membrane also leads to damage to the architecture of seminiferous tubules, resulting in the loss of the central lumen as well as testicular atrophy [62,63]. Similarly, our results showed a reduction in seminiferous tubule size, as well as seminiferous epithelium degeneration or the absence of some germ cell types (particularly primary spermatocytes) in both ZIKV-infected groups. Of note, some of those parameters were exacerbated in the presence of 4G2. Several studies have considered that Sertoli cells are a key target for ZIKV infection in the testes [59,62,64]. Our data suggest that ZIKV maintains its tropism to these somatic cells, once a reduction of Sertoli cell efficiency was observed in our experimental model. Another possible consequence associated with Sertoli cell alterations caused by ZIKV infection was a

Fig. 7. Therapeutic administration of an antiviral peptide (AH-D) ameliorate CZS outcomes. Schematic representation of experimental strategy to evaluate the antiviral activity of AH-D peptide in ADE of maternal ZIKV infection model (a). C57BL/6 pregnant mice were injected with PBS (black bar or circles) or 10^6 PFU/mouse of Brazilian ZIKV strain (HS-2015-BA-01) on embryonic day 5.5 in the presence (green bar or triangles) of monoclonal pan-flavivirus antibody (4G2). AH-D therapy started at three days post infection (blue bar or lozenges) until ED 15.5, when foetuses and placentas were harvested and weighted (d-e), foetal malformations were registered (c), and ZIKV RNA was quantified by qRT-PCR in foetal brain (b). qRT-PCR results are expressed as the median of ZIKV RNA copies per mg of sample tissue. Weight data are expressed as the median and are representative of at least two independent experiments. *, p < .05 vs. PBS controls, † p < .05 vs. 4G2 + ZIKV, as assessed by Mann-Whitney test (b) and one-way ANOVA followed by Newman-Keuls post-test (d-e).

reduction in the meiotic index, which indicates that Sertoli cells were not fully supporting the development of germ cells. On the other hand, decreased testosterone levels associated with diminished 3β-HSD+ Leydig cells population have been reported in acute ZIKV infection [59,62]. In this study, no substantial morphometric alterations were observed for Leydig cells, suggesting that these steroidogenic cells could not serve as a primary target for ZIKV within the vertically infected testes.

Arthrogryposis is a common feature of congenital ZIKV infection [10,65]. Here, we demonstrated that ZIKV infection augmented generation of osteoclasts and osteoblasts, suggesting an increased bone remodelling profile. The findings also revealed an increase in osteoclasts and osteocytes numbers, without change in the osteoblasts of ZIKV-infected offspring. This result suggests impaired osteoblast differentiation induced by ZIKV, which resulted in increased bone loss. As an underlying mechanism, we found increased expression of IL-6 cytokine and RANKL/OPG ratio in the femur of ZIKV-infected mice. Increased levels of those mediators are directly associated with bone reabsorption [66]. Accordingly, a study conducted by Bayless and colleagues [67] demonstrated that ZIKV infects cranial neural crest cells, which are the direct progenitors of bone cells and may underlie ZIKV-associated microcephaly.

We have recently engineered a brain-penetrating peptide (AH-D) that exhibits antiviral activity against ZIKV and other mosquito-borne viruses [16,68]. Using the adult A129 model of ZIKV infection, we demonstrated that therapeutic administration of AH-D peptide protected ZIKV-infected mice against mortality and significantly reduced clinical symptoms, viral loads, and neuroinflammation, as well as reduced the levels of microgliosis, neurodegeneration, and brain damage. Here, we further evaluated the therapeutic efficacy of AH-D peptide during congenital ZIKV infection in an immunocompetent mouse model. Our results revealed that AH-D peptide therapy prevented ZIKV RNA detection in the brain of the offspring and also reduced the number of malformed embryos. Compared to protective strategies [69,70] aimed at post-exposure treatment (one hour to one day post-infection), the AH-D peptide therapy was effective when started at later stages

(three days post-infection) and resulted in complete suppression of detectable viral loads in the brains of all pups. As such, the AH-D peptide therapy demonstrates the potential of addressing two key challenges associated with ZIKV infection: 1) transport across intact BBB leading to suppression of viral replication in ZIKV-infected brains and 2) therapeutic inhibition of CZS effects in the offspring of pregnant ZIKV-infected mice. Although AH-D peptide treatment prevented ZIKV infection in foetal brain and reduced foetal mortality, it could not completely rescue ZIKV-induced birth defects, suggesting that host responses unleashed by infection are also important during ZIKV pathogenesis. In this context, it will be important to evaluate whether the combination of neuroprotective drugs and antiviral drugs could become an optimal treatment for CZI.

In conclusion, our results reveal that congenital ZIKV infection induces severe birth defects in offspring from the embryonic phase until adulthood. Those consequences are potentiated by ADE and associated with enhanced MIA. Altogether, the results suggest that MIA and ADE are possible mechanisms involved in the generation of CZS and provide further insights into the long-term consequences of early maternal ZIKV infection and outcomes of congenital ZIKV infection in adulthood. Finally, our results suggest that antiviral treatments, such as AH-D peptide therapy, may be beneficial during early maternal ZIKV infection.

Funding

Biology at Nanyang Technological University. Funders had no role in study design, data collection, data analysis, interpretation of data, or writing of the report.

Author contributions

V.N.C., N.-J.C, A.C.P.O., M.M.T, V.V.C. and D.G.S. planned the studies. V.N.C., G. F., D.C.M., V.T.S., C.M.Q-J, A.L.B.M., A.F.A.F., C.D.F.S., T.P.M., V.F.Q., A.C.F.D., K.T.O.S., I.P., A.L.C.V.R., L.C.S., F.A.G.M., N.T.W., M.A.P.O., S.M., T.S., G.P.G., conducted experiments. V.N.C., G.F., D.C.M., V.T.S., C.M.Q-J., A.F.A.F., K.T.O.S., S.M., G.P.G., J.A.J., F.M.S., M.F.D.M., E.M.A.M.M, F.M.R., G.M.J.C., A.L.T., N.-J.C., A.C.P.O., M.M.T, V.V.C., D.G.S. interpreted the results. V.N.C., G.F., V.T.S., A.F.A.F., S.M., J.A.J., F.M.S., F.M.R., G.M.J.C., N.-J.C, A.C.P.O., M.M.T., V.V.C., D.G.S. wrote the first draft of the paper. F.M.R., N.-J.C, M.M.T., V.V.C., D.G.S. obtained funding. All authors reviewed, edited and approved the paper.

Appendix A. Supplementary data

Supplementary data to this article can be found online at https://doi.org/10.1016/j.ebiom.2019.05.014.

References

[1] Brasil P, Pereira JP, Moreira ME, et al. Zika virus infection in pregnant women in Rio de Janeiro. N Engl J Med 2016;375:2321–34.

[2] Moore CA, Staples JE, Dobyns WB, et al. Characterizing the pattern of anomalies in congenital zika syndrome for pediatric clinicians. JAMA Pediatr 2017;171:288–95.

[3] Hoen B, Schaub B, Funk AL, et al. Pregnancy outcomes after ZIKV infection in French territories in the Americas. N Engl J Med 2018;378:985–94.

[4] Estes ML, McAllister AK. Maternal immune activation: implications for neuropsychiatric disorders. Science (80-) 2016;353:772–7.

[5] Knuesel I, Chicha L, Britschgi M, et al. Maternal immune activation and abnormal brain development across CNS disorders. Nat Rev Neurol 2014;10:643–60.

[6] Butler D. Brazil asks whether Zika acts alone to cause birth defects. Nature 2016;535:475–6.

[7] Polonio CM, de Freitas CL, Zanluqui NG, Peron JPS. Zika virus congenital syndrome: experimental models and clinical aspects. J Venom Anim Toxins Incl Trop Dis 2017;23:1–9.

[8] Mahalingam S, Teixeira MM, Halstead SB. Zika enhancement: a reality check. Lancet Infect Dis 2017;17:686–8.

[9] Costa VV, Fagundes CT, Valadão DF, et al. Subversion of early innate antiviral responses during antibody-dependent enhancement of dengue virus infection induces severe disease in immunocompetent mice. Med Microbiol Immunol 2014;203:231–50.

[10] Xavier-Neto J, Carvalho M, Pascoalino B dos S, et al. Hydrocephalus and arthrogryposis in an immunocompetent mouse model of ZIKA teratogeny: a developmental study. PLoS Negl Trop Dis 2017;11:1–29.

[11] Radyushkin K, Hammerschmidt K, Boretius S, et al. Neuroligin-3-deficient mice: model of a monogenic heritable form of autism with an olfactory deficit. Genes Brain Behav 2009;8:416–25.

[12] De Castro BM, Pereira GS, Magalhães V, et al. Reduced expression of the vesicular acetylcholine transporter causes learning deficits in mice. Genes Brain Behav 2009;8:23–35.

[13] Funchal C, Dani C. Neurociências: Modelos Experimentais Em Animais. Porto Alegre: EdiPUCRS, Editora Universitária Metodista; 2014.

[14] da Silveira VT, Medeiros D de C, Ropke J, et al. Effects of early or late prenatal immune activation in mice on behavioral and neuroanatomical abnormalities relevant to schizophrenia in the adulthood. Int J Dev Neurosci 2017;58:1–8.

[15] Bitanihirwe BKY, Peleg-Raibstein D, Mouttet F, Feldon J, Meyer U. Late prenatal immune activation in mice leads to behavioral abnormalities relevant to the negative symptoms of schizophrenia. Schizophr Res 2010;117:273–4.

[16] Jackman JA, Costa VV, Park S, et al. Therapeutic treatment of Zika virus infection using a brain-penetrating antiviral peptide. Nat Mater 2018:1.

[17] Doria JG, de Souza JM, Silva FR, et al. The mGluR5 positive allosteric modulator VU0409551 improves synaptic plasticity and memory of a mouse model of Huntington's disease. J Neurochem 2018;147:222–39.

[18] Schmued LC, Stowers CC, Scallet AC, Xu L. Fluoro-jade C results in ultra high resolution and contrast labeling of degenerating neurons. Brain Res 2005;1035:24–31.

[19] Foureaux G, Franca JR, Nogueira JC, et al. Ocular inserts for sustained release of the angiotensin-converting enzyme 2 activator, diminazene aceturate, to treat glaucoma in rats. PLoS One 2015;10:1–18.

[20] Costa GMJ, Lacerda SMSN, Figueiredo AFA, Leal MC, Rezende-Neto JV, França LR. Higher environmental temperatures promote acceleration of spermatogenesis in vivo in mice (Mus musculus). J Therm Biol 2018. https://doi.org/10.1016/j.jtherbio.2018.07.010.

[21] Johnson L, Neaves WB. Age-related changes in the Leydig cell population, seminiferous tubules and sperm production in stallions. Biol Reprod 1981;24:703–12.

[22] Abercrombie M. Estimation of nuclear population from microtome sections. Anat Rec 1946. https://doi.org/10.1002/ar.1090940210.

[23] Amann RP. Reproductive capacity of dairy bulls. IV. Spermatogenesis and testicular germ cell degeneration. Am J Anat 1962;110:69–78.

[24] Ramos-Vara JA. Technical aspects of immunohistochemistry. Vet Pathol 2005. https://doi.org/10.1354/vp.42-4-405.

[25] Macari S, Sharma LA, Wyatt A, et al. Lactation induces increases in the RANK/RANKL/OPG system in maxillary bone. Bone 2018;110:160–9.

[26] Rathore APS, Saron WAA, Lim T, Jahan N, St John AL. Maternal immunity and antibodies to dengue virus promote infection and Zika virus–induced microcephaly in fetuses. Sci Adv 2019;5 [eaav3208].

[27] Meyer U. Prenatal poly(I:C) exposure and other developmental immune activation models in rodent systems. Biol Psychiatry 2014;75:307–15.

[28] Graham AM, Rasmussen JM, Rudolph MD, et al. Maternal systemic Interleukin-6 during pregnancy is associated with Newborn amygdala phenotypes and subsequent behavior at 2 years of age. Biol Psychiatry 2018;83:109–19.

[29] Rudolph MD, Graham AM, Feczko E, et al. Maternal IL-6 during pregnancy can be estimated from newborn brain connectivity and predicts future working memory in offspring. Nat Neurosci 2018:1–8.

[30] Smith SEP, Li J, Garbett K, Mirnics K, Patterson PH. Maternal immune activation alters Fetal brain development through Interleukin-6. J Neurosci 2007;27:10695–702.

[31] Paul LM, Carlin ER, Jenkins MM, et al. Dengue virus antibodies enhance Zika virus infection. Clin Transl Immunol 2016;5:e117.

[32] Castanha PMS, Nascimento EJM, Braga C, et al. Enhancement of Zika infection by dengue-specific antibodies does not alter the production of interleukin 6 in FcγRII-expressing K562 cells. J Infect Dis 2017;216:614–5.

[33] Hueston L, Ramirez R, Mahalingam S. Enhancement of Zika infection by dengue virus-specific antibody is associated with low levels of antiviral factors. J Infect Dis 2017;216:612–4.

[34] Dejnirattisai W, Supasa P, Wongwiwat W, et al. Dengue virus sero-cross-reactivity drives antibody-dependent enhancement of infection with zika virus. Nat Immunol 2016;17:1102–8.

[35] Rogers TF, Goodwin EC, Briney B, et al. Zika virus activates de novo and cross-reactive memory B cell responses in dengue-experienced donors. Sci Immunol 2017;2:eaan6809.

[36] Bardina SV, Bunduc P, Tripathi S, et al. Enhancement of Zika virus pathogenesis by preexisting antiflavivirus immunity. Science (80-) 2017;356:175–80.

[37] McCracken MK, Gromowski GD, Friberg HL, et al. Impact of prior flavivirus immunity on Zika virus infection in rhesus macaques. PLoS Pathog 2017;13:1–22.

[38] Pantoja P, Pérez-Guzmán EX, Rodríguez IV, et al. Zika virus pathogenesis in rhesus macaques is unaffected by pre-existing immunity to dengue virus. Nat Commun 2017;8. https://doi.org/10.1038/ncomms15674.

[39] Terzian ACB, Schanoski AS, De Oliveira Mota MT, et al. Viral load and cytokine response profile does not support antibody-dependent enhancement in dengue-primed Zika virus-infected patients. Clin Infect Dis 2017;65:1260–5.

[40] Wen J, Elong Ngono A, Angel Regla-Nava J, et al. Dengue virus-reactive CD8+T cells mediate cross-protection against subsequent Zika virus challenge. Nat Commun 2017;8. https://doi.org/10.1038/s41467-017-01669-z.

[41] Ribeiro GS, Kikuti M, Tauro LB, et al. Does immunity after Zika virus infection cross-protect against dengue? Lancet Glob Health 2018;6:e140–1.

[42] Rodriguez-Barraquer I, Costa F, Nascimento EJM, et al. Impact of preexisting dengue immunity on Zika virus emergence in a dengue endemic region. Science (80-) 2019;363:607–10.

[43] Gilmore JH, Jarskog LF, Vadlamudi S, Lauder JM. Prenatal infection and risk for schizophrenia: IL-1β, IL-6, and TNFα inhibit cortical neuron dendrite development. Neuropsychopharmacology 2004;29:1221–9.

[44] Cugola FR, Fernandes IR, Russo FB, et al. The Brazilian Zika virus strain causes birth defects in experimental models. Nature 2016;534:267–71.

[45] Hirsch AJ, Roberts VHJ, Grigsby PL, et al. Zika virus infection in pregnant rhesus macaques causes placental dysfunction and immunopathology. Nat Commun 2018;9. https://doi.org/10.1038/s41467-017-02499-9.

[46] Dudley DM, Van Rompay KK, Coffey LL, et al. Miscarriage and stillbirth following maternal Zika virus infection in nonhuman primates. Nat Med 2018;24:1104–7.

[47] de Araújo TVB, de Alencar Ximenes RA, de Barros Miranda Filho D, et al. Association between microcephaly, Zika virus infection, and other risk factors in Brazil: final report of a case-control study. Lancet Infect Dis 2018;18:328–36.

[48] Miner JJ, Cao B, Govero J, et al. Zika virus infection during pregnancy in mice causes placental damage and Fetal demise. Cell 2016;165:1081–91.

[49] Satterfield-Nash A, Kotzky K, Allen J, et al. Health and development at age 19–24 months of 19 children who were born with microcephaly and laboratory evidence of congenital Zika virus infection during the 2015 Zika virus outbreak — Brazil, 2017. MMWR Morb Mortal Wkly Rep 2017;66:1347–51.

[50] Nem de Oliveira Souza I, Frost PS, França JV, et al. Acute and chronic neurological consequences of early-life Zika virus infection in mice. Sci Transl Med 2018;10 [eaar2749].

[51] Li C, Xu D, Ye Q, et al. Zika virus disrupts neural progenitor development and leads to microcephaly in mice. Cell Stem Cell 2016;19:120–6.

[52] Shi Y, Li S, Wu Q, et al. Vertical transmission of the Zika virus causes neurological disorders in mouse offspring. Sci Rep 2018;8:1–14.

[53] Wu KY, Zuo GL, Li XF, et al. Vertical transmission of Zika virus targeting the radial glial cells affects cortex development of offspring mice. Cell Res 2016;26: 645–54.

[54] Julander JG, Siddharthan V, Park AH, et al. Consequences of in utero exposure to Zika virus in offspring of AG129 mice. Sci Rep 2018;8:9384.

[55] de Paula Freitas B, Ko AI, Khouri R, et al. Glaucoma and congenital Zika syndrome. Ophthalmology 2017;124:407–8.

[56] Yepez JB, Murati FA, Pettito M, et al. Ophthalmic manifestations of congenital Zika syndrome in Colombia and Venezuela. JAMA Ophthalmol 2017;135:440–5.

[57] Mohr EL, Block LN, Newman CM, et al. Ocular and uteroplacental pathology in a macaque pregnancy with congenital Zika virus infection. PLoS One 2018;13: 1–28.

[58] Strange DP, Green R, Siemann DN, Gale M, Verma S. Immunoprofiles of human Sertoli cells infected with Zika virus reveals unique insights into host-pathogen crosstalk. Sci Rep 2018;8:1–15.

[59] Stassen L, Armitage C, van der Heide D, Beagley K, Frentiu F. Zika virus in the male reproductive tract. Viruses 2018;10:198.

[60] Robinson CL, Chong ACN, Ashbrook AW, et al. Male germ cells support long-term propagation of Zika virus. Nat Commun 2018;9:1–11.

[61] Spencer JL, Lahon A, Tran LL, et al. Replication of Zika virus in human prostate cells: a potential source of sexually transmitted virus. J Infect Dis 2017. https://doi.org/10. 1093/infdis/jix436.

[62] Govero J, Esakky P, Scheaffer SM, et al. Zika virus infection damages the testes in mice. Nature 2016;540:438–42.

[63] Shan C, Muruato AE, Jagger BW, et al. A single-dose live-attenuated vaccine prevents Zika virus pregnancy transmission and testis damage. Nat Commun 2017;8. https:// doi.org/10.1038/s41467-017-00737-8.

[64] Kumar A, Jovel J, Lopez-Orozco J, et al. Human sertoli cells support high levels of zika virus replication and persistence. Sci Rep 2018;8:1–11.

[65] Alvino ACMI, de Mello LRM, de Oliveira JDAMM. Association of arthrogryposis in neonates with microcephaly due to Zika virus - a case serie. Rev Bras Saúde Matern Infant 2016;16:S83–8.

[66] Shim JH, Stavre Z, Gravallese EM. Bone loss in rheumatoid arthritis: basic mechanisms and clinical implications. Calcif Tissue Int 2018;102:533–46.

[67] Bayless NL, Greenberg RS, Swigut T, Wysocka J, Blish CA. Zika virus infection induces cranial neural crest cells to produce cytokines at levels detrimental for neurogenesis. Cell Host Microbe 2016;20:423–8.

[68] Jackman JA, Shi P-Y, Cho N-J. Targeting the Achilles heel of mosquito-borne viruses for antiviral therapy. ACS Infect Dis 2018;5:4–8 [acsinfecdis.8b00286].

[69] Sapparapu G, Fernandez E, Kose N, et al. Neutralizing human antibodies prevent Zika virus replication and fetal disease in mice. Nature 2016;540:443–7.

[70] Yu Y, Deng YQ, Zou P, et al. A peptide-based viral inactivator inhibits Zika virus infection in pregnant mice and fetuses. Nat Commun 2017;8. https://doi.org/10.1038/ ncomms15672.